J Physiol 590.24 (2012) pp 6327–6342

The Journal of Physiology

Distinct localization and modulation of $Ca_v1.2$ and $Ca_v1.3$ L-type Ca^{2+} channels in mouse sinoatrial node

Carl J. Christel[1], Natalia Cardona[1], Pietro Mesirca[2,3,4], Stefan Herrmann[5], Franz Hofmann[6], Joerg Striessnig[7], Andreas Ludwig[5], Matteo E. Mangoni[2,3,4] and Amy Lee[1]

[1] *Department of Molecular Physiology and Biophysics, University of Iowa, IA, USA*
[2] *CNRS, UMR-5203, Institut de Génomique Fonctionnelle, Département de Physiologie, LabEx ICST, Montpellier, F-34094, France*
[3] *INSERM, U661, Montpellier, F-34094, France*
[4] *Universités de Montpellier 1 & 2, UMR-5203, Montpellier, F-34094, France*
[5] *Institut für Experimentelle und Klinische Pharmakologie und Toxikologie, Friedrich-Alexander-Universität Erlangen-Nürnberg, Germany*
[6] *Institut für Pharmakologie und Toxikologie, Technische Universität München*
[7] *Department of Pharmacology and Toxicology, Institute of Pharmacy, Center for Molecular Biosciences, University of Innsbruck, Austria*

Key points

- In the sinoatrial node (SAN), Ca_v1 voltage-gated Ca^{2+} channels mediate L-type currents that are essential for normal cardiac pacemaking.
- Both $Ca_v1.2$ and $Ca_v1.3$ Ca^{2+} channels are expressed in the SAN but how their distinct properties affect cardiac pacemaking is unknown.
- Here, we show that unlike $Ca_v1.2$, $Ca_v1.3$ undergoes voltage-dependent facilitation and colocalizes with ryanodine receptors in sarcomeric structures.
- By mathematical modelling, these properties of $Ca_v1.3$ can improve recovery of pacemaking after pauses and stabilize SAN pacemaking during excessively slow heart rates.
- We conclude that voltage-dependent facilitation and colocalization with ryanodine receptors distinguish $Ca_v1.3$ from $Ca_v1.2$ channels in the SAN and contribute to the major impact of $Ca_v1.3$ on pacemaking.

Abstract Dysregulation of L-type Ca^{2+} currents in sinoatrial nodal (SAN) cells causes cardiac arrhythmia. Both $Ca_v1.2$ and $Ca_v1.3$ channels mediate sinoatrial L-type currents. Whether these channels exhibit differences in modulation and localization, which could affect their contribution to pacemaking, is unknown. In this study, we characterized voltage-dependent facilitation (VDF) and subcellular localization of $Ca_v1.2$ and $Ca_v1.3$ channels in mouse SAN cells and determined how these properties of $Ca_v1.3$ affect sinoatrial pacemaking in a mathematical model. Whole cell Ba^{2+} currents were recorded from SAN cells from mice carrying a point mutation that renders $Ca_v1.2$ channels relatively insensitive to dihydropyridine antagonists. The $Ca_v1.2$-mediated current was isolated in the presence of nimodipine (1 μM), which was subtracted from the total current to yield the $Ca_v1.3$ component. With strong depolarizations (+80 mV), $Ca_v1.2$ underwent significantly stronger inactivation than $Ca_v1.3$. VDF of $Ca_v1.3$ was evident during recovery from inactivation at a time when $Ca_v1.2$ remained inactivated. By immunofluorescence, $Ca_v1.3$ colocalized with ryanodine receptors in sarcomeric structures while $Ca_v1.2$ was largely restricted to the delimiting plasma membrane. $Ca_v1.3$ VDF enhanced recovery of pacemaker activity after pauses and positively regulated pacemaking during slow heart rate in a numerical model of mouse SAN automaticity, including preferential coupling of $Ca_v1.3$ to ryanodine receptor-mediated Ca^{2+} release. We conclude that strong VDF and colocalization with

DOI: 10.1113/jphysiol.2012.239954

ryanodine receptors in mouse SAN cells are unique properties that may underlie a specific role for $Ca_v1.3$ in opposing abnormal slowing of heart rate.

(Received 5 July 2012; accepted after revision 2 October 2012; first published online 8 October 2012)
Corresponding author A. Lee: Department of Molecular Physiology and Biophysics, University of Iowa, 5–610 Bowen Science Building 51 Newton Road, Iowa City, IA 52242, USA. Email: amy-lee@uiowa.edu

Abbreviations AP, action potential; BB, blocking buffer; Ca_v, voltage-gated Ca^{2+} channel; CDF, Ca^{2+}-dependent facilitation; CDI, Ca^{2+}-dependent inactivation; DHP, dihydropyridine; PDZ, post-synaptic density/zonula occludens; HCN4KiT-Cre, double transgenic mice with targeted deletion of $Ca_v1.2$ in the SAN; KB, K^+ buffer; LCS, low calcium solution; NIM, nimodipine; PM, plasma membrane; RYR, ryanodine receptor; SAN, sinoatrial node; SANDD, SAN dysfunction and deafness syndrome; SR, sarcoplasmic reticulum; VDF, voltage-dependent facilitation; VDI, voltage-dependent inactivation; WT, wild-type.

Introduction

Normal cardiac rhythmicity depends on the intrinsic properties, modulation and subcellular localization of ion channels in the heart. Voltage-gated Ca_v1 channels ($Ca_v1.2$ and $Ca_v1.3$) mediate L-type Ca^{2+} currents ($I_{Ca,L}$) that play distinct roles in different cardiac cell types. Expressed throughout the heart, $Ca_v1.2$ regulates action potential (AP) duration and excitation–contraction coupling in the ventricle (Klugbauer *et al.* 2002). $Ca_v1.3$ is largely absent from the ventricles but is highly expressed in atria, atrioventricular node and sinoatrial node (SAN) (Marger *et al.* 2011; Zhang *et al.* 2011). Loss-of-function of $Ca_v1.3$ both in mice and humans causes 'sick sinus' syndrome characterized by severe bradycardia (Platzer *et al.* 2000; Le Scouarnec *et al.* 2008; Baig *et al.* 2011). Thus, factors that regulate $Ca_v1.3$ may have a major impact on pacemaking.

Compared to $Ca_v1.2$, $Ca_v1.3$ activates more rapidly and at more negative membrane potentials (Koschak *et al.* 2001; Xu & Lipscombe, 2001). These properties allow $Ca_v1.3$ to contribute more significantly than $Ca_v1.2$ to the diastolic depolarization in SAN cells (Mangoni *et al.* 2006*a*). However, $Ca_v1.3$ differs in other ways from $Ca_v1.2$ that may further determine the larger impact of $Ca_v1.3$ on sinoatrial pacemaking. In transfected HEK293T cells, $Ca_v1.3$ undergoes significantly greater Ca^{2+}-dependent inactivation (CDI) and less voltage-dependent inactivation (VDI) than $Ca_v1.2$ (Tadross *et al.* 2010). In addition, $Ca_v1.3$ interacts selectively with multiple post-synaptic density/zonula occludens (PDZ) domain containing proteins that regulate the function and localization of these channels in various cell types. For example, harmonin controls $Ca_v1.3$ current density by enhancing ubiquitination and proteosomal degradation of these channels in auditory hair cells (Gregory *et al.* 2011). Interactions with Shank in neurons allows for $Ca_v1.3$ modulation by G-protein coupled receptors and coupling to cAMP response element-binding protein-dependent transcription (Olson *et al.* 2005; Zhang *et al.* 2005, 2006). Erbin and densin promote voltage- and Ca^{2+}-dependent facilitation (CDF) (Calin-Jageman *et al.* 2007; Jenkins *et al.* 2010), respectively, of $Ca_v1.3$ but not $Ca_v1.2$. Whether such $Ca_v1.3$-specific modulation occurs in SAN cells is unknown but necessary for understanding the privileged role of $Ca_v1.3$ in regulating heart rhythm.

The absence of pharmacological agents that unequivocally distinguish between $Ca_v1.2$ and $Ca_v1.3$ poses a major challenge to the characterization of these Ca_v1 channels in their native contexts. However, genetically modified mice ($Ca_v1.2$ DHP) in which a single point mutation eliminates the high sensitivity of $Ca_v1.2$ to dihydropyridines (DHPs), have proven useful in this regard (Sinnegger-Brauns *et al.* 2004). Thus, in cells from $Ca_v1.2$ DHP mice that express both $Ca_v1.2$ and $Ca_v1.3$, DHP antagonists spare the $Ca_v1.2$-mediated L-type current. In whole cell patch-clamp recordings from SAN cells isolated from these mice, we identified voltage-dependent properties that distinguish $Ca_v1.2$ and $Ca_v1.3$. In addition, we uncovered differences in the subcellular localization of $Ca_v1.2$ and $Ca_v1.3$ in SAN cells by immunofluorescence. In a mathematical model of mouse SAN cells, we demonstrate how these unique properties of $Ca_v1.3$ may be physiologically relevant in controlling pacemaking.

Methods

Ethical approval

All procedures involving animals were approved by the Institutional Animal Care and Use Committee at the University of Iowa, University of Erlangen, and the University of Montpellier. These procedures were in accordance with National Institutes of Health guidelines.

Preparation of isolated mouse sinoatrial node cells

SAN cells were isolated from 2- to 6-month-old male or female $Ca_v1.2$ DHP mice (Sinnegger-Brauns *et al.* 2004). Age-matched wild-type (WT) mice were used as controls. Mice were anaesthetized by inhalation of

isoflurane and depth of anaesthesia assessed by loss of hindlimb reflex. Beating hearts were removed from anaesthetized animals and immediately transferred to pre-warmed (37°C) Tyrode solution (in mM: 140 NaCl, 5 Hepes, 5.4 KCl, 1.8 $CaCl_2$, 1 $MgCl_2$, 5.5 glucose, pH 7.35 with NaOH). The SAN was removed and washed with low Ca^{2+} solution (LCS; in mM: 140 NaCl, 5 Hepes, 5.4 KCl, 0.2 $CaCl_2$, 0.5 $MgCl_2$, 5.5 glucose, 1.2 KH_2PO_4, 50 taurine, 1 mg ml^{-1} bovine serum albumin, pH 6.9 with NaOH), cut into 10–20 fragments, and then incubated in LCS containing proteases (in U ml^{-1}: 229 collagenase, 1.9 elastase (both Worthington Biochemical, Lakewood, NJ, USA), 0.9 protease type XIV (Sigma-Aldrich, St. Louis, MO, USA), pH 6.9 with NaOH) at 37°C for 20–25 min, shaken gently every 5 min. The tissue was washed three times with high K^+ buffer (KB, in mM: 100 potassium glutamate, 5 Hepes, 20 glucose, 25 KCl, 10 potassium aspartate, 2 $MgSO_4$, 10 KH_2PO_4, 20 taurine, 5 creatine, 0.5 EGTA, pH 7.35 with KOH). The tissue was triturated to release SAN cells, which were kept at 4°C until experiments performed the same day.

Electrophysiological recordings

Isolated SAN cells (in KB) were transferred to a glass coverslip in a recording chamber and left to settle for 15–20 min before recording. Upon wash-in of Tyrode solution, rhythmically beating SAN cells were identified for recording. Glass recording electrodes (2–4 MΩ) were filled with intracellular solution containing (in mM: 135 $CsCl_2$, 10 Hepes, 10 EGTA, 1 $MgCl_2$, 4 Mg-ATP, pH 7.2 with CsOH). After establishing whole cell configuration Tyrode solution was replaced with extracellular recording solution (in mM: 130 TEA-Cl, 1 $MgCl_2$, 25 Hepes, 4 $BaCl_2$, 10 4-aminopyridine, pH 7.3 with TEA-OH). Holding voltage was set to −60 mV. Currents were recorded with an EPC-9 patch-clamp amplifier using PULSE software by HEKA Electronics (Lambrecht/Pfalz, Germany). Leak and capacitive transients were calculated and subtracted using a *P*/4 protocol. Data were analysed using IGOR Pro software (WaveMetrics, Lake Oswego, OR, USA). Averaged data represent mean ± standard error of the mean.

Generation of sinoatrial node-specific $Ca_V1.2$ knockout mice

Double transgenic mice with targeted deletion of $Ca_v1.2$ in the SAN ($Ca_V1.2^{flox/flox}$, $HCN4^{KiTCre/+}$) were generated by crossing floxed $Ca_V1.2$ (Seisenberger *et al.* 2000) and HCN4KiT-Cre (Hoesl *et al.* 2008). Cre-mediated recombination was induced by administration of tamoxifen (1 mg 25 mg^{-1}, I.P.) for five consecutive days.

Immunofluorescence

Isolated SAN cells in KB solution were left to settle for 30 min on glass-bottom microwell dishes (35 mm Petri dish, 14 mm microwell) coated with fibronectin (0.05 $\mu g\ \mu l^{-1}$ in Ham's F-10 media). Cells were fixed with 2% paraformaldehyde for 15 min, washed three times with phosphate-buffered saline (PBS), and blocked for 1 h in blocking buffer (BB: 0.075% Triton-X 100, 5% goat serum, in PBS). To block non-specific sites, cells were incubated with rabbit IgG (1:50 in BB) overnight at 4°C and after washing three times with PBS (15 min each), cells were incubated with goat anti-rabbit Fab fragments (1:25 in BB) for 2 h at room temperature. Cells were washed and incubated overnight at 4°C with the appropriate primary antibodies diluted in BB: mouse-anti-ryanodine receptor (RYR) type 2 (1:1000, Thermo Scientific, Waltham, MA, USA), rabbit polyclonal antibodies against $Ca_v1.2$ (1:2000; Tippens *et al.* 2008) or $Ca_v1.3$ (1:500; Gregory *et al.* 2011). The specificity of these antibodies for labelling $Ca_v1.2$ and $Ca_v1.3$ in SAN was confirmed using tissue and cells from mice lacking either channel (Supplementary Fig. 1). In some experiments, commercially available rabbit polyclonal $Ca_v1.3$ antibodies (Alomone Labs, Jerusalem, Israel) were used, which produced qualitatively similar results as the $Ca_v1.3$ antibodies we characterized previously (Gregory *et al.* 2011). Following washes, cells were incubated with secondary antibodies (Alexa 488 goat-antirabbit and Alexa 568 goat-anti-mouse, 1:1000 in BB) for 2 h at room temperature, washed three times with PBS and mounted on glass microscope slides with Dako fluorescence mounting medium (Carpinteria, CA, USA). Images were acquired with a Fluoview (FV1000, Olympus) confocal microscope on an upright microscope (BX61WI) using a 100× oil-immersion objective. Line scan analysis of immunofluorescence intensity (Fig. 5) was performed with Fluoview software (Olympus).

Quantitation of colocalization within a selected region of interest was performed with the JACoP plug-in for ImageJ (Bolte & Cordelieres, 2006). To restrict analysis to colocalization of Ca_v1 and RYR2 labelling within the plasma membrane and sarcomeric structures, the signal threshold intensity for both was manually set to levels that just eliminated fluorescence signals outside these regions. Use of the Costes automatic threshold calculation tended to overestimate colocalization as it included signal intensities outside plasma and sarcomeric membranes. Using the manually set thresholds, Mander's colocalization coefficient was determined by the JACoP software. This coefficient varied from 0 to 1, the former corresponding to non-overlapping signals and the latter reflecting 100% colocalization between the two fluorophores. As Mander's colocalization coefficient depends on the accuracy with which the threshold is determined, Pearson's correlation coefficient was also measured,

which is generally insensitive to inaccuracies of the threshold setting. Similar results were obtained with both procedures.

To compare the subcellular distribution of colocalized RYR2 with $Ca_v1.2$ or $Ca_v1.3$, we performed three line scans per cell through RYR-labelled sarcomeric structures. The signal from each line scan was subdivided into plasma membrane and intracellular signals and the ratio of the two was calculated as the relative intensity. Using this method, a plasma membrane/intracellular ratio of 1 would indicate similar signal intensities in both areas. A ratio less than 1 would signify greater intracellular compared to plasma membrane labelling and vice versa for a ratio greater than 1 (Supplementary Fig. 2).

Computational analysis

We performed numerical simulations of pacemaker activity by modifying a model of mouse SAN automaticity that we developed previously (Mangoni *et al.* 2006*b*). This previous model fairly reproduced the behaviour of membrane-bound ion channels and automaticity of mouse SAN pacemaker cells; however, it did not include calculation of intracellular ion homeostasis and compartments underlying Ca^{2+} handling (Mangoni *et al.* 2006*b*). To generate a new model of mouse SAN cell automaticity calculating Ca^{2+} handling, we used the set of model equations in Mangoni *et al.* (2006*b*) to simulate the behaviour of ion channels of the plasma membrane and added calculations of intracellular compartments and ion concentrations according to Kurata *et al.* (2002). The general structure of the model, including the organization of intracellular Ca^{2+} handling compartments and membrane-bound ion channels and RYRs, is shown in Supplementary Fig. 3.

The volumes of the subsarcolemmal space, as well as that of sarcoplasmic reticulum (SR) and non-SR compartments were defined as in Kurata *et al.* (2002). Intracellular Na^+ and K^+ concentrations, as well as Ca^{2+} handling were also calculated according to Kurata *et al.* (2002). We used the set of equations previously published by Maltsev & Lakatta (2009) to calculate RYR-dependent Ca^{2+} release from the SR. To simulate co-distribution between $Ca_v1.3$ channels and RYRs, our model assumed that 71% of the total $Ca_v1.3$-mediated $I_{Ca,L}$ current density contributed to the Ca^{2+} concentration of the subsarcolemmal compartment (SS_{Ca}). The residual 29% of $Ca_v1.3$-mediated $I_{Ca,L}$, the $Ca_v1.2$-mediated $I_{Ca,L}$, $Ca_v3.1$-mediated $I_{Ca,T}$ and background Ca^{2+} current ($I_{b(Ca)}$) contributed to Ca^{2+} of the bulk cytosol ($[Ca^{2+}]_i$) (Kurata *et al.* 2002; Maltsev & Lakatta, 2009), as well as to Ca^{2+} load of the SR network (Maltsev & Lakatta, 2009). Consequently, $Ca_v1.2$- and $Ca_v3.1$-dependent Ca^{2+} entries did not control RYR-dependent Ca^{2+} release directly. In this respect, our model differs from that of Kurata *et al.* (2002) and Kharche *et al.* (2011), which assume that $Ca_v1.3$- and $Ca_v1.2$-mediated $I_{Ca,L}$ as well as $Ca_v3.1$-mediated $I_{Ca,T}$ contribute to SS_{Ca} and can collectively trigger RYR-dependent Ca^{2+} release. All the other parameters controlling membrane-bound ion channel densities and ionic pumps were set as in the model by Mangoni *et al.* (2006*b*).

To calculate VDF of $Ca_v1.3$ channels we modelled VDF by directly modifying the equations generating $Ca_v1.3$-mediated $I_{Ca,L}$ in the mouse SAN automaticity model. Indeed, we reasoned that during simulations of pacemaker activity, the preceding AP amplitude would condition $Ca_v1.3$- and $Ca_v1.2$-mediated $I_{Ca,L}$ similarly to the prepulse in a voltage-clamp experiment, while the diastolic interval would determine the time after the prepulse. As we calculated the VDF model parameters by fitting the dependency of VDF from the prepulse amplitude and time after prepulse in voltage-clamp experiments conducted on native SAN cells we expected that the model would reproduce the behaviour of $Ca_v1.3$- and $Ca_v1.2$-mediated $I_{Ca,L}$ at different SAN cell firing rates. Specifically, to compute $Ca_v1.3$-mediated $I_{Ca,L}$, we assumed that the probability of $Ca_v1.3$ to be in the open state is the result of combined effects of VDF, VDI and CDI. VDF of $Ca_v1.3$-dependent Ca^{2+} current ($I_{Ca,L}$) was modelled by adding a variable for VDF, $f(f)$, that affected $I_{Ca,L}$ independently from VDI and CDI according to the equations:

$$I_{Ca,L} = g_{max}(V - V_{rev})f\,(d)f\,(I)f\,(\mathrm{Ca})f\,(f\,)$$

$$f\,(f\,) = (1 + (F(v) + F(t))/100)$$

$$F(v) = A\,\exp^{(BV)}$$

$$F(t) = C(A_2 + (A_1 - A_2)/(1 + \exp^{(A_3 - t)/s)},$$

where g_{max} is the maximal current conductance, V is the membrane voltage, V_{rev} is the current reversal potential, t is the time, $f(d)$ is the activation variable, $f(I)$ and $f(Ca)$ are the inactivation variables corresponding to VDI and CDI respectively, $F(v)$ is the dependence of VDF on the prepulse voltage (Fig. 2*A*, Supplementary Fig. 3*A*) and $F(t)$ is the dependence of VDF on the recovery interval (Figs 2*B* and S3*B*). A, B, A_1, A_2 and A_3 are constant factors; s is a slope factor. The $f(f)$ variable was omitted in calculations of $Ca_v1.2$-mediated $I_{Ca,L}$ activation (Fig. 1, this study) and inactivation (Mangoni *et al.* 2003) time constants experimentally measured in SAN cells were used to model $Ca_v1.3$-mediated $I_{Ca,L}$. The maximal conductance of $Ca_v1.3$- and $Ca_v1.2$-mediated $I_{Ca,L}$ was set according to measurements in extracellular 2 mM Ca^{2+} native SAN cells (Mangoni *et al.* 2003). The model satisfactorily reproduced our experimental characterization of $Ca_v1.3$ VDF (Figs 2 and 6). We

assumed that SS_{Ca} directly controlled the open probability of RYRs and the CDI inactivation variable $f(Ca)$ of $Ca_v1.3$-mediated $I_{Ca,L}$. This assumption is experimentally verified (Neco *et al.* 2012; see below). In the main code of the SAN model we added an expression to apply simulated voltage commands when needed. The user in simulations of cellular automaticity can deactivate this function.

Slowing of pacemaking was obtained by simulating activation of the ATP-dependent K^+ current (I_{KATP}). I_{KATP} is expressed in mouse SAN pacemaker cells and is activated by lowering the intracellular ATP concentration during ischaemia (Fukuzaki *et al.* 2008). Calculations were performed in the Jsim environment for integration of differential equations (http://nsr.bioeng.washington.edu/jsim/). The integration step was set to 200 μs. Simulations were analysed using the Graph Prism software (ver. 5.03).

Results

Cells dissociated from the SAN of $Ca_v1.2$ DHP mice exhibited properties similar to those described previously for mouse SAN cells (Mangoni & Nargeot, 2001). The cells selected for recording were generally spindle-shaped (Fig. 1*A*) and were spontaneously beating in physiological saline (Tyrode's solution). Similar to values reported previously for mouse primary pacemaker SAN cells (Mangoni & Nargeot, 2001), the mean capacitance of $Ca_v1.2$ DHP SAN cells was 32.4 ± 1.6 pA pF^{-1} ($n = 23$). Compared to WT SAN cells, $Ca_v1.2$ DHP SAN cells exhibited a similar range of I_{Ba} densities (5–33 pA pF^{-1} for $Ca_v1.2$ DHP *vs.* 12–33 pA pF^{-1} for WT), which was consistent with previous results indicating that $Ca_v1.2$ current density was not significantly altered by the DHP knock-in mutation (Sinnegger-Brauns *et al.* 2004; Zhang *et al.* 2007).

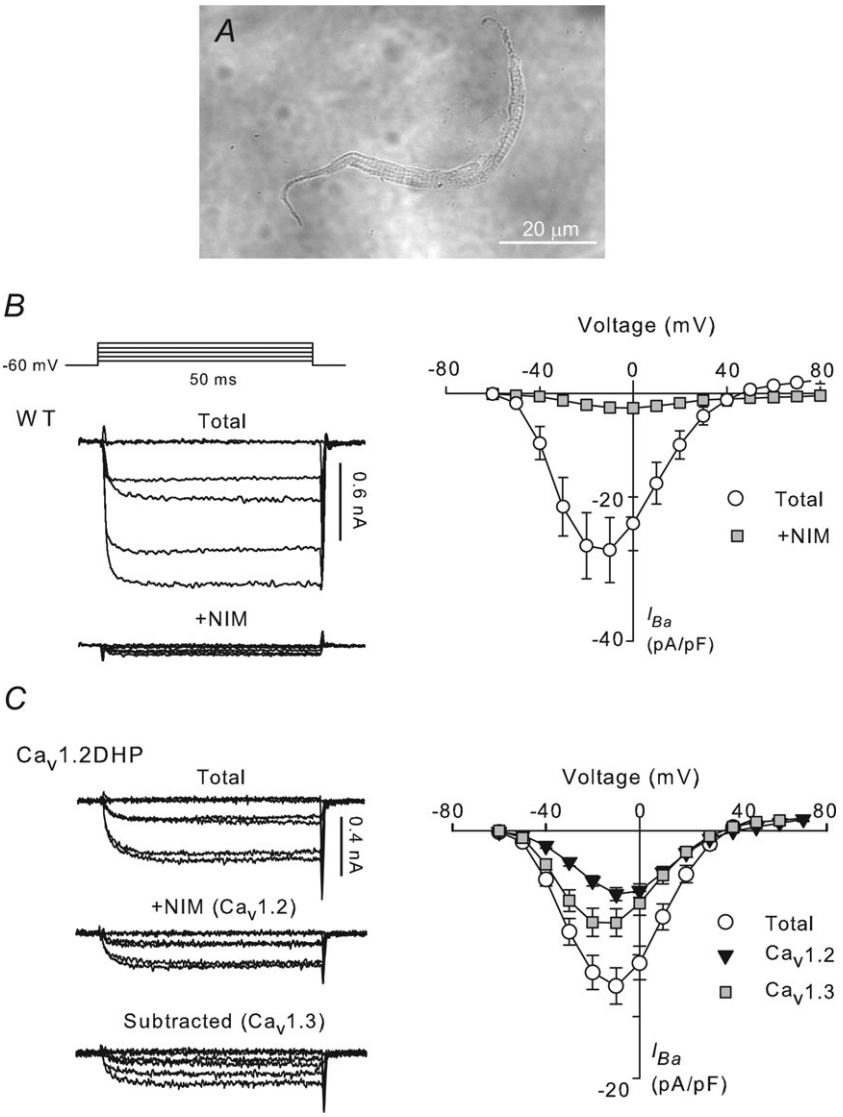

Figure 1. Pharmacological isolation of I_{Ba} mediated by $Ca_v1.2$ and $Ca_v1.3$ in $Ca_v1.2$ DHP mouse sinoatrial node (SAN) cells
A, phase contrast image of a representative mouse SAN cell used for whole cell patch-clamp recordings. *B*, effects of nimodipine (NIM, 1 μM) on I_{Ba} in wild-type (WT, $n = 3$) mouse SAN cells. *C*, same as in *B* except with $Ca_v1.2$ DHP SAN cells ($n = 23$). The residual current in the presence of NIM ($Ca_v1.2$) was subtracted from the total current to yield the $Ca_v1.3$ component. In *B* and *C*, representative I_{Ba} traces and voltage protocol (left) and current–density (pA pF^{-1}) *vs.* voltage (mV) relation (right) are shown.

In the present study, we focused on Ba^{2+} currents (I_{Ba}) rather than Ca^{2+} currents (I_{Ca}) to restrict our analysis to voltage- rather than Ca^{2+}-dependent modulation of Ca_v1 channels (Christel & Lee, 2012 for review). To isolate I_{Ba} mediated by $Ca_v1.2$ and $Ca_v1.3$ in $Ca_v1.2$ DHP SAN cells, we used nimodipine (NIM, 1 μM) a DHP antagonist of Ca_v1 channels. In SAN cells from WT mice, NIM nearly abolished I_{Ba} (up to 95%, Fig. 1*B*), consistent with the dominant contribution of $Ca_v1.2$ and $Ca_v1.3$ channels to the whole cell L-type current in these cells (Mangoni *et al.* 2003; Marionneau *et al.* 2005). In contrast, the same concentration of NIM reduced I_{Ba} only ~58% in $Ca_v1.2$ DHP SAN cells, which was consistent with a reduced sensitivity of $Ca_v1.2$ DHP channels to NIM (Fig. 1*C*). We interpreted the residual current that was not blocked by NIM as largely mediated by $Ca_v1.2$. Subtraction of this NIM insensitive I_{Ba} from total I_{Ba} yielded the $Ca_v1.3$ component (Fig. 1*C*).

The presence of a modest DHP-insensitive component (~5%) of the whole cell I_{Ba} in WT SAN cells (Fig. 1*B*) could be problematic if it contributed more significantly to I_{Ba} in $Ca_v1.2$ DHP cells as it would be interpreted as '$Ca_v1.2$' using our NIM subtraction protocol. However, if this protocol effectively dissected Ca_v1 components of I_{Ba}, the properties of the NIM-insensitive current and the difference current should match those expected of $Ca_v1.2$ and $Ca_v1.3$, respectively. For example, in heterologous expression systems, $Ca_v1.3$ activates more rapidly and at more negative voltages than $Ca_v1.2$ (Koschak *et al.* 2001; Scholze *et al.* 2001; Xu & Lipscombe, 2001). In our experiments, Boltzmann fits of current–voltage relations revealed that compared to $Ca_v1.2$ currents, $Ca_v1.3$ currents activated at more negative voltages ($V_{1/2} = -25.4 \pm 1.4$ mV for $Ca_v1.3$ *vs.* -15.7 ± 1.4 mV for $Ca_v1.2$; $n = 22$, $P < 0.001$) in $Ca_v1.2$ DHP SAN cells (Fig. 1*C*). To compare the activation kinetics of $Ca_v1.2$ and $Ca_v1.3$ currents, we fit the rising phase of I_{Ba} evoked by various voltages with a single exponential function. With this analysis, $Ca_v1.3$ currents activated significantly faster than $Ca_v1.2$ currents (up to 30%, $P < 0.01$; Fig. 2*A*). Based on findings that recombinant $Ca_v1.3$ channels undergo less VDI than $Ca_v1.2$ (Koschak *et al.* 2001), we also compared inactivation of $Ca_v1.2$ and $Ca_v1.3$ I_{Ba}. For these experiments, a long (500 ms) test pulse was used to evoke I_{Ba} and time constants for inactivation determined from a single exponential fit of the I_{Ba} decay. As expected, $Ca_v1.3$ currents inactivated significantly more slowly (~36% at -10 mV, $P = 0.01$; Fig. 2*B*) than $Ca_v1.2$. Taken together,

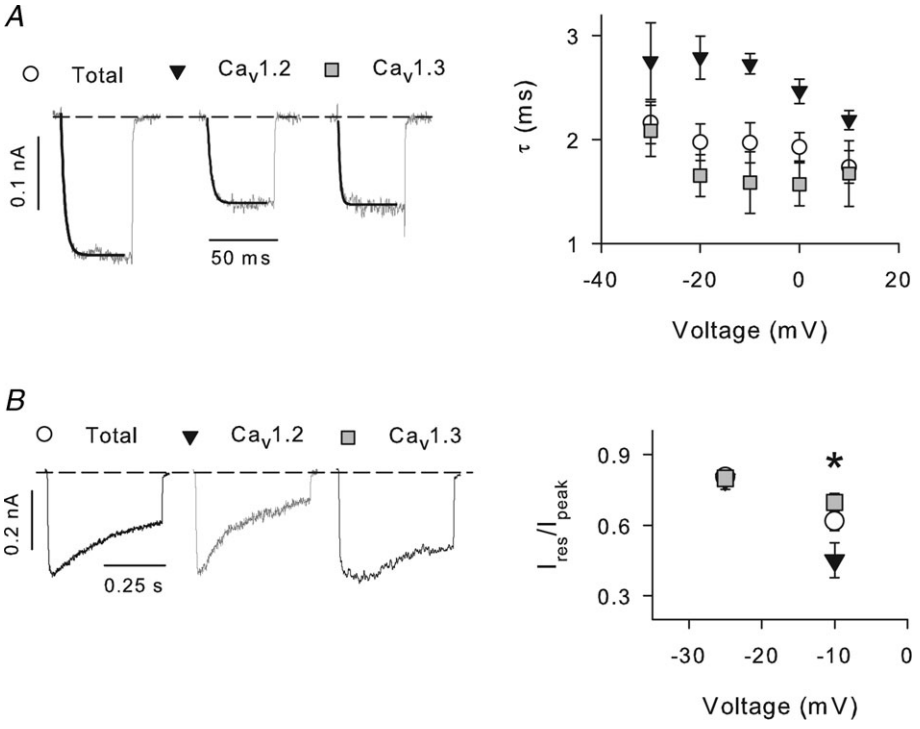

Figure 2. $Ca_v1.3$ currents activate faster and inactivate more slowly than $Ca_v1.2$ currents in mouse sinoatrial node cells
A, $Ca_v1.2$ and $Ca_v1.3$-mediated I_{Ba} was evoked and isolated as in Fig. 1*B*. Current traces (left) were fit with a single exponential function (smooth black line). The resulting time constants (τ) were plotted against test voltage (right, $n = 22$). *B*, inactivation of I_{Ba} evoked by 500 ms test pulses to a test voltage of -10 mV. I_{res}/I_{peak} = current amplitude at the end of the pulse normalized to peak amplitude, plotted for test voltages of -30 and -10 mV. $^*P = 0.01$, one-way ANOVA, $n = 8$.

these results validated our strategy for isolating $Ca_v1.2$ and $Ca_v1.3$ from the total I_{Ba} in $Ca_v1.2$ DHP SAN cells, which was applied for the remainder of the study.

We have shown previously that $Ca_v1.3$ channels in transfected HEK293T cells undergo voltage-dependent facilitation (VDF) (Calin-Jageman *et al.* 2007). Because L-type currents in rabbit SAN cells also undergo VDF, we tested if VDF was a property of $Ca_v1.2$ and/or $Ca_v1.3$ in mouse SAN cells. Using a modified voltage protocol for measuring VDF, we compared I_{Ba} evoked before (P1) and after (P2) a conditioning prepulse (Fig. 3). VDF due to the conditioning prepulse should manifest as an increase in the P2 compared to P1 current. Rather than facilitation, both Ca_v1 currents exhibited VDI in that the P2 current amplitude was always less than that for P1 (Fig. 3). Consistent with our kinetic analyses (Fig. 2*B*), VDI was significantly weaker for $Ca_v1.3$ compared to $Ca_v1.2$ (~26% at +80 mV prepulse voltage, $P < 0.001$). Notably, the ratio of P2/P1 current amplitude was relatively invariant with prepulse voltage except for between +60 and +80 mV, where P2/P1 for $Ca_v1.3$ significantly increased (Fig. 3). This suggested that VDF might have been occluded by VDI such that overt VDF was not observed with this protocol.

To follow-up on this possibility, we sought to resolve VDF from VDI by measuring I_{Ba} during recovery from inactivation. The rationale for this approach was based on our previous findings that Ca_v channels may recover faster from inactivation than facilitation, such that facilitation can be measured once channels have fully recovered from inactivation (Lee *et al.* 1999, 2000). For these experiments, we compared P2 and P1 current amplitudes at varying intervals after a conditioning prepulse to +80 mV. Consistent with a role for $Ca_v1.3$ VDF in offsetting the effects of VDI, the full amplitude of the $Ca_v1.3$ current was restored within ~250 ms of the prepulse, at which time the $Ca_v1.2$ current was still ~20% inactivated. At longer recovery intervals (~450 ms), $Ca_v1.3$ showed small but measurable VDF (~5%) while $Ca_v1.2$ currents remained ~15% inactivated (Fig. 4). These results demonstrate that $Ca_v1.3$ channels in mouse SAN cells undergo VDF, a property that is not shared by $Ca_v1.2$.

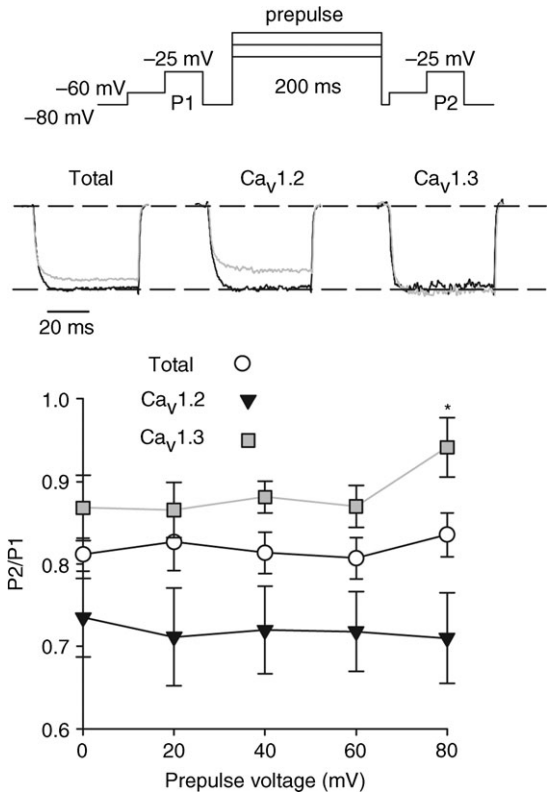

Figure 3. $Ca_v1.3$ and $Ca_v1.2$ undergo VDI in mouse sinoatrial node (SAN) cells
Top, voltage protocol. Test currents were evoked by 50 ms test pulses before (P1) and after (P2) a 200 ms conditioning prepulse. Middle, representative I_{Ba} evoked by P1 (black trace) and P2 (grey trace). Bottom, fractional current (P2/P1) was plotted against prepulse voltage. *$P < 0.001$, two-way ANOVA for group and voltage, Tukey *post hoc* test, $n = 9$.

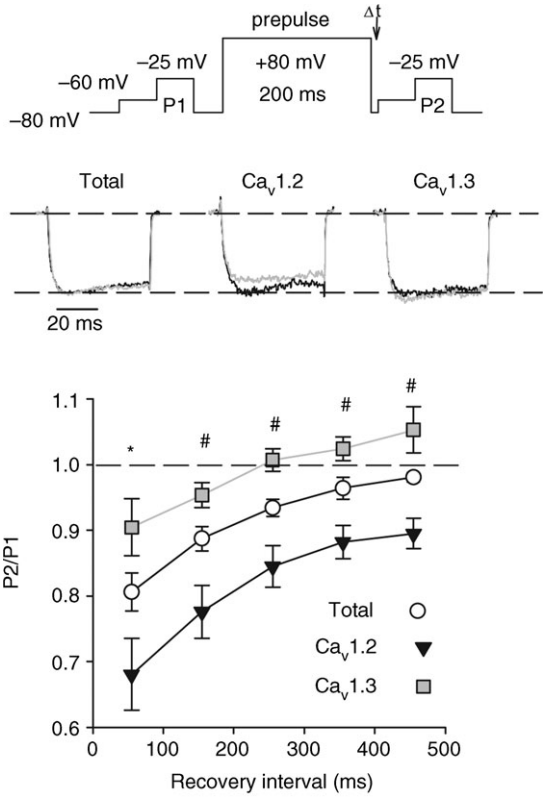

Figure 4. $Ca_v1.3$ but not $Ca_v1.2$ undergoes voltage-dependent facilitation during recovery from inactivation
Top, voltage protocol. Test currents were evoked by 50 ms test pulses before (P1) and at variable intervals (Δt) after (P2) a 200 ms conditioning prepulse to +80 mV. Middle, representative I_{Ba} evoked by P1 (black trace) and P2 (grey trace). Bottom, fractional current was plotted against prepulse to P2 interval. *$P < 0.01$, #$P < 0.001$ for $Ca_v1.3$ *vs.* $Ca_v1.2$ by one-way ANOVA and Tukey *post hoc* test, $n = 8$.

In addition to differences in their intrinsic properties and regulation, distinct localization of $Ca_v1.2$ and $Ca_v1.3$ may also affect their respective contributions to SAN function. Therefore, we compared the subcellular distribution of $Ca_v1.2$ and $Ca_v1.3$ in isolated mouse SAN cells. We used $Ca_v1.2$ and $Ca_v1.3$ antibodies, which we have shown to specifically recognize the corresponding channels in rodent brain (Tippens *et al.* 2008; Gregory *et al.* 2011). To verify that these antibodies are equally specific for immunofluorescence of mouse SAN, we compared immunostaining in tissue obtained from WT mice and those lacking $Ca_v1.3$ (Platzer *et al.* 2000) or $Ca_v1.2$. As full body knockout of $Ca_v1.2$ causes embryonic lethality (Seisenberger *et al.* 2000), we used mice with inducible, targeted deletion of $Ca_v1.2$ in the SAN (see Methods section). In both fixed SAN tissue and isolated SAN cells, there was strong immunofluorescence corresponding to $Ca_v1.2$ and $Ca_v1.3$ antibodies in samples obtained from WT but not knockout mice (Supplementary Fig. 1). These results validated the use of these antibodies for reporting the localization of $Ca_v1.2$ or $Ca_v1.3$ in SAN cells.

In isolated SAN cells, $Ca_v1.3$ but not $Ca_v1.2$ antibodies labelled distinct bands of regular periodicity (Supplementary Fig. 1, Fig. 5), a pattern resembling the localization of RYR2 reported in SAN cells (Rigg *et al.* 2000). As in ventricular myocytes, RYRs mediate Ca^{2+}-induced Ca^{2+} release in SAN cells (Rigg *et al.* 2000; Bogdanov *et al.* 2001), which subsequently could depend on Ca^{2+} influx through $Ca_v1.3$ channels. To determine if $Ca_v1.3$ colocalized with RYR2, we performed double labelling with mouse monoclonal anti-RYR2 antibodies and either $Ca_v1.2$ (Fig. 5*A*–*E*) or $Ca_v1.3$ (Fig. 5*F*–*J*)

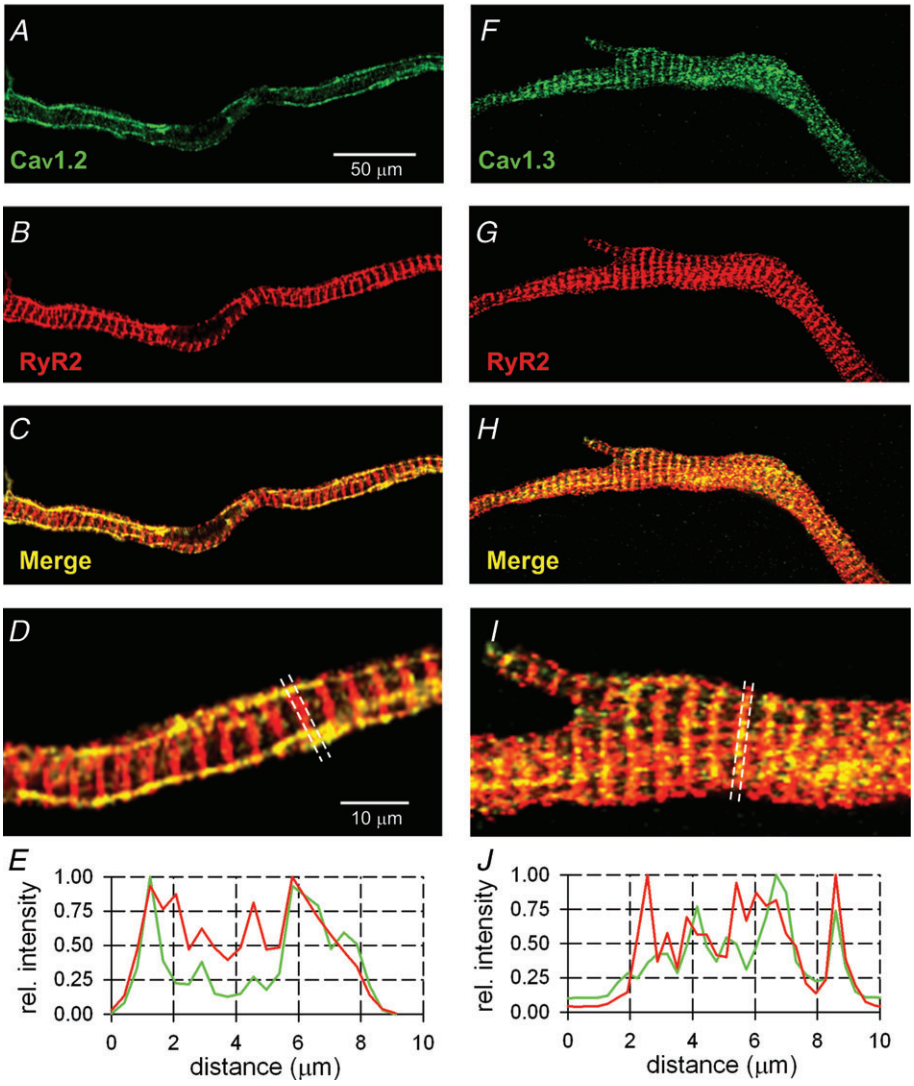

Figure 5. Confocal micrographs showing double labelling of RYR2 and $Ca_v1.2$ (*A*–*E*) or $Ca_v1.3$ (*F*–*J*)
Regions of colocalization are yellow in the merged images (*C*, *D*, *H* and *I*). *E* and *J*, line scan analysis through region marked with dashed lines in *D* and *I* showing signals for RYR2 (red) and $Ca_v1.2$ or $Ca_v1.3$ (green).

antibodies. Both $Ca_v1.2$ and $Ca_v1.3$ were strongly colocalized with RYR2 based on coefficients for Mander's overlap (0.71 ± 0.08 for $Ca_v1.3$ and 0.85 ± 0.07 for $Ca_v1.2$, $n = 3$ each) and Pearson's correlation (0.74 ± 0.09 for $Ca_v1.3$, 0.71 ± 0.01 for $Ca_v1.2$). Unexpectedly, $Ca_v1.3$ strongly colocalized with RYR2 both at the sarcolemma and in the sarcomeric structures, while $Ca_v1.2$ mainly colocalized with RYR2 in the sarcolemmal membrane. Line scan analyses confirmed the coincidence of $Ca_v1.3$ and RYR2 immunofluorescence throughout the SAN cell (Fig. 5*J*), while $Ca_v1.2$ labelling most intensely overlapped with RYR2 at the delimiting sarcolemmal membrane (Fig. 5*E*).

To quantitatively estimate the difference in the subcellular distribution of $Ca_v1.2$ and $Ca_v1.3$, we calculated the ratio of plasma membrane to intracellular Ca_v1 immunofluorescence from line scans through RYR2-labelled sarcomeric structures (see Methods and Supplementary Fig. 2). By this metric, values less than 1 indicate greater signal intensity in intracellular compared to plasma membrane regions. This analysis indicated stronger intensity of $Ca_v1.3$ labelling in sarcomeric structures than on the plasma membrane (ratio $= 0.86 \pm 0.03$, $n = 3$). In contrast, $Ca_v1.2$ labelling was far more intense on the plasma membrane than intracellularly (ratio $= 2.44 \pm 0.10$, $n = 3$). When compared to values obtained for RYR2 (ratio $= 0.95 \pm 0.04$ and 0.99 ± 0.04 for $Ca_v1.3$ and $Ca_v1.2$ double-labelled groups, respectively), only the ratio obtained for $Ca_v1.2$ was significantly different from that of $Ca_v1.3$ and RYR2 ($P < 0.001$ by ANOVA and *post-hoc* Bonferroni test). Taken together, these results verify a distinct subcellular distribution of Ca_v1 channels and suggest that $Ca_v1.3$ is better positioned than $Ca_v1.2$ to promote RYR Ca^{2+} release in mouse SAN cells.

The unique localization and VDF exhibited by $Ca_v1.3$ and not $Ca_v1.2$ could significantly influence the important role of $Ca_v1.3$ in SAN pacemaking (Mangoni *et al.* 2003). Furthermore, no pharmacological or molecular tools are currently available to selectively inhibit VDF of $Ca_v1.3$ channels, a condition that prevents direct experimental investigation of the physiological role of VDF in cardiac pacemaker activity. Computational models have proven useful in predicting the impact of alterations in ionic currents on mouse SAN pacemaking (Mangoni *et al.* 2006*b*). To predict the impact of VDF on pacemaker activity, we thus used a numerical model of mouse SAN automaticity. We assumed that $Ca_v1.3$ VDF operates on channel gating in a way that is independent from VDI, CDI, and CDF. Experimental evidence showed that enhanced RYR-dependent Ca^{2+} release promotes CDI of SAN $I_{Ca,L}$ in a mouse model of congenital polymorphic ventricular tachycardia (Neco *et al.* 2012). Consequently, we assumed that RYRs also contributed with $Ca_v1.3$-mediated $I_{Ca,L}$ to the subsarcolemmal Ca^{2+} concentration, which in turn directly controlled CDI.

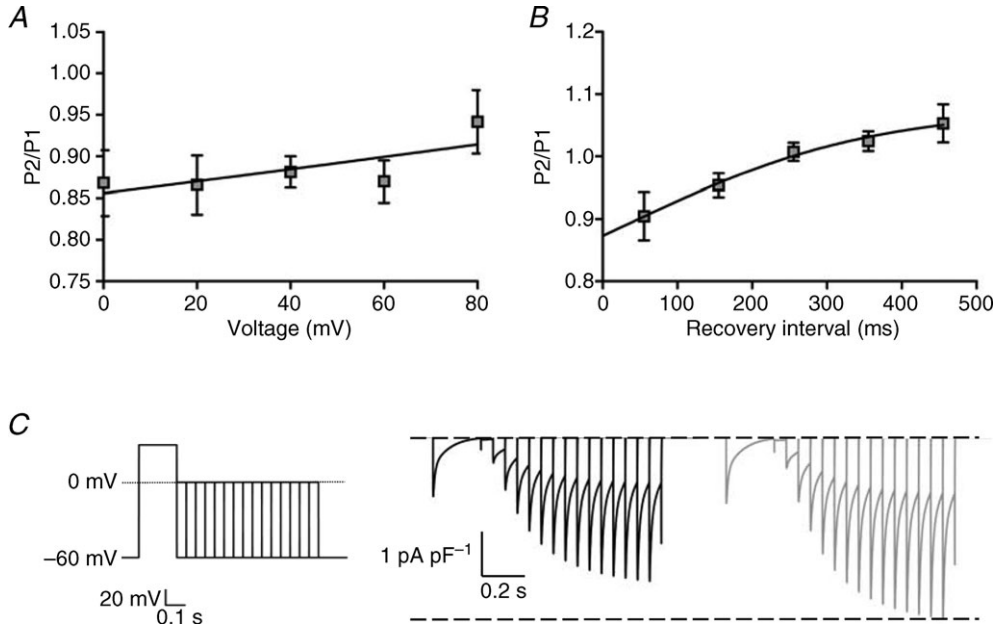

Figure 6. Numerical modelling of VDF in mouse sinoatrial node cells
A and *B*, fitting by the model of P2/P1 ratio as a function of the conditioning prepulse voltage (*A*) or recovery interval (*B*). Voltage protocols were the same as in Figs. 3 and 4. *C*, simulation of voltage-clamp experiments showing recovery from inactivation of $Ca_v1.3$-mediated $I_{Ca,L}$ with (grey line) or without (black line) voltage-dependent facilitation. Dashed lines indicate zero current level and maximal $I_{Ca,L}$ during recovery from inactivation. For the voltage-clamp protocol (left), the 200 ms conditioning prepulse was set to +30 mV.

As $Ca_v1.3$ channels preferentially colocalized with RYR2 in comparison to $Ca_v1.2$ channels (Fig. 5), the model included $Ca_v1.3$-mediated $I_{Ca,L}$ as the main contributor of Ca^{2+} entry in the subsarcolemmal space. By quantitative analyses of our colocalization data (Fig. 5), we estimated ~71% of total $Ca_v1.3$ immunofluorescence colocalized with that for RYRs. Therefore, we assumed that 71% of $Ca_v1.3$ channels contributed to subsarcolemmal Ca^{2+} concentration coupled to RYR-dependent Ca^{2+} release and that the remaining 29% contributed mainly to cytoplasmic Ca^{2+} concentration along with $Ca_v1.2$ and $Ca_v3.1$ channels (see Methods).

The model satisfactorily fitted experimental data on VDF of $Ca_v1.3$-mediated $I_{Ca,L}$ as a function of prepulse amplitude or recovery time (Fig. 6*A* and *B*). In voltage-clamp simulations, we simulated $Ca_v1.3$-mediated $I_{Ca,L}$ with a prepulse amplitude to +30 mV, a voltage close to the maximum positive voltage reached by the simulated SAN AP. $Ca_v1.3$-mediated $I_{Ca,L}$ was then measured at 0 mV (Fig. 6*C*). Simulations of voltage-clamp experiments

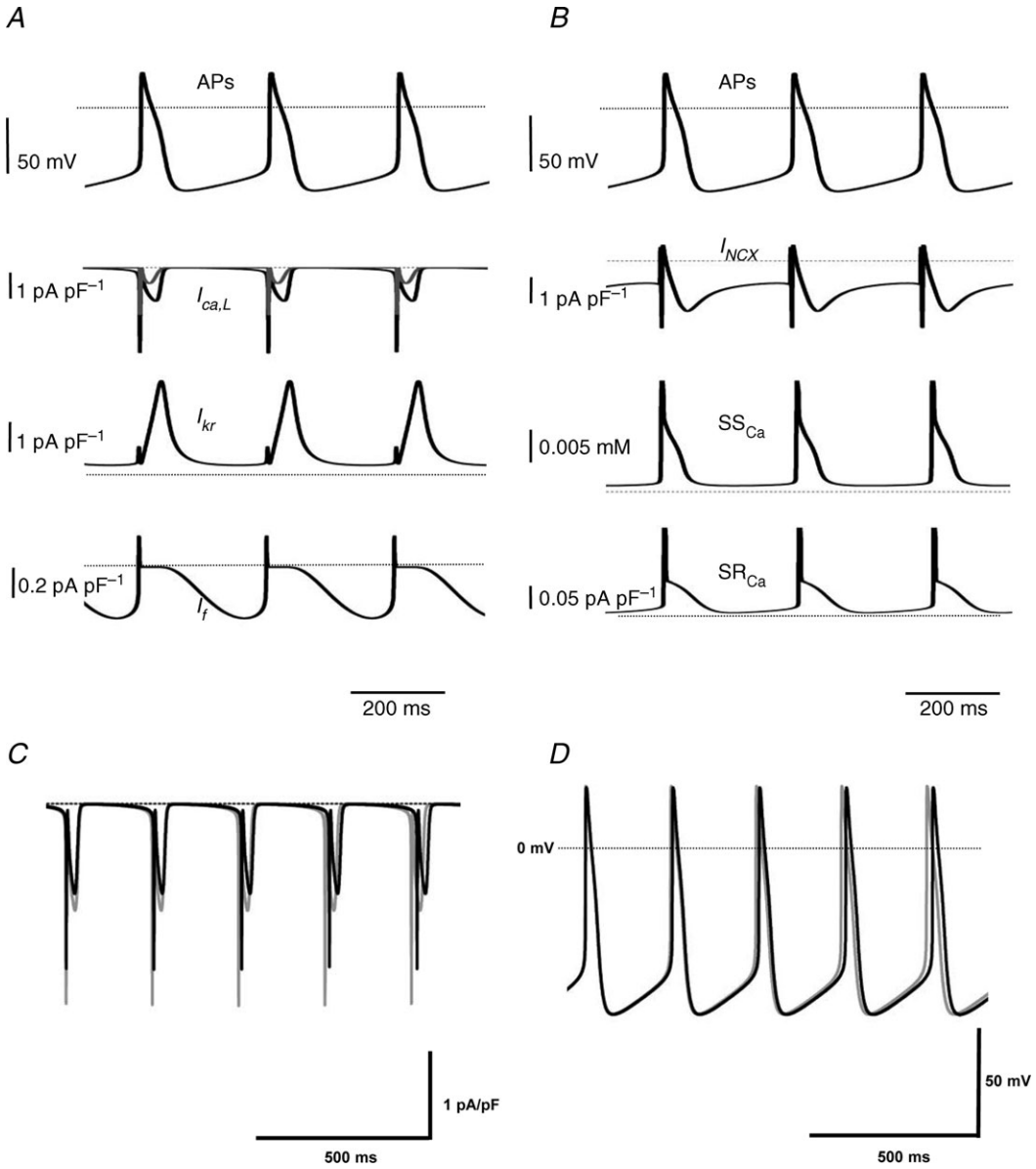

Figure 7. Effects of $Ca_v1.3$ voltage-dependent facilitation (VDF) on $I_{Ca,L}$ and sinoatrial node (SAN) cell pacemaking in a mathematical model
A, numerical simulations, including $Ca_v1.3$ VDF of SAN action potentials (APs), $I_{Ca,L}$ ($Ca_v1.3$, black line; $Ca_v1.2$-mediated, grey line), I_{Kr}, and I_f. *B*, comparison between pacemaker activity (APs), Na^+/Ca^{2+} exchanger current (I_{NCX}), subsarcolemmal Ca^{2+} concentration (SS_{Ca}), and SR Ca^{2+} release (SR_{Ca}) in our model. *C*, $Ca_v1.3$-mediated $I_{Ca,L}$ calculated with VDF (grey line) or without VDF (black line). *D*, corresponding pacemaker activity with VDF (grey line) or without VDF (black line).

showed that VDF increased $Ca_v1.3$-mediated $I_{Ca,L}$ during recovery from inactivation (Fig. 6*C*). Consistently with our experimental findings (Fig. 4), $Ca_v1.3$-mediated $I_{Ca,L}$ amplitude was higher in the model containing VDF for each recovery time tested (from 14.2% at 66 ms, to 23.8% at 800 ms recovery time).

The numerical model of mouse SAN pacemaker activity, which included VDF and preferential coupling of $Ca_v1.3$ channels to RYRs, faithfully reproduced SAN APs and the main ionic currents involved in the diastolic depolarization (Fig. 7*A*). The hyperpolarization-activated current I_f was activated in the first phase of the diastolic depolarization and its density increased in parallel with the decay of I_{Kr} (Fig. 7*A*). The fast Na^+ current (I_{Na}) was modelled as the sum of the tetrodotoxin-sensitive and tetrodotoxin-insensitive component as previously described (Lei *et al.* 2004; Mangoni *et al.* 2006*b*). The density of I_{Na} during diastolic depolarization was similar to that of $Ca_v1.3$-mediated $I_{Ca,L}$ (data not shown). $Ca_v1.3$-mediated $I_{Ca,L}$ began to activate about midway between the maximum diastolic potential and the threshold of the following AP upstroke, while the $Ca_v1.2$-mediated $I_{Ca,L}$ was activated during the AP upstroke (Fig. 7*A*). In comparison to a model excluding $Ca_v1.3$ channel VDF, $Ca_v1.3$-mediated $I_{Ca,L}$ density was increased (25%) at a basal diastolic interval of 278 ms (Fig. 7*C* and *D*). As a consequence of augmented $Ca_v1.3$-mediated $I_{Ca,L}$ during pacemaking (Fig. 7*C*), the model predicted a small but measurable positive chronotropic effect on basal pacing rate compared to a model lacking VDF (2%; Fig. 7*D*).

To gain further insights into the potential impact of VDF in regulating aberrant pacemaking, we modelled the behaviour of $Ca_v1.3$-mediated $I_{Ca,L}$ upon slowing of pacemaker activity by activation of currents through K_{ATP} channels (I_{KATP}, see Methods; Fig. 8*A* and *B*). I_{KATP} inhibits SAN automaticity, which may protect against myocardial damage due to ischemic insults (Fukuzaki *et al.* 2008). In rabbit SAN cells, pharmacological activation of I_{KATP} robustly slows pacemaking. Arrest of automaticity can also be observed at high I_{KATP} densities (Fukuzaki *et al.* 2008). We thus modelled the impact of I_{KATP} activation by moderately increasing K_{ATP} conductance (0.1–0.15 pA pF^{-1} in the diastolic depolarization range). The effect of I_{KATP} activation was a transient pause in automaticity that recovered to regular steady-state pacemaking. However, pacemaker activity recovered faster in the model with VDF (within 828 ms; Fig. 8*A*) than without VDF (within 2005 ms; Fig. 8*B*). During the first beat upon recovery of pacemaking, $Ca_v1.3$-mediated $I_{Ca,L}$ was 36.2% larger in the model with VDF than without VDF (Fig. 8*C*–*E*). After recovery of automaticity, steady-state pacemaker activity was slower than in control simulations with no I_{KATP} activation in the model including VDF and excluding VDF. Compared to control conditions, steady-state pacemaker activity was slowed by 18% in the model including VDF and by 20% in the model excluding VDF (from 278 to 338 ms including VDF and from 283 to 350 ms excluding VDF; Fig. 8*G*), which would constitute a significant reduction in heart rate *in vivo*. At steady state, $Ca_v1.3$-mediated $I_{Ca,L}$ was 17% larger in the model including VDF than in the model excluding VDF (Fig. 8*F*), which is consistent with a role for VDF in promoting full recovery from inactivation (Figs 4 and 6). Slowing of pacemaker activity itself induces recovery of $I_{Ca,L}$ from inactivation, which increases $Ca_v1.3$-mediated $I_{Ca,L}$ even without VDF (44%; Fig. 8*H*). However, with VDF, slowing of pacemaking was reduced and pacemaker activity was measurably faster (3.4%) than that of the model excluding VDF (Fig. 8*G*). Taken together, our results demonstrate that $Ca_v1.3$ VDF may operate as a positive chronotropic factor that may regulate Ca^{2+} signals and excitability of SAN cells.

Discussion

Our study provides multiple lines of evidence for the functional specialization of Ca_v1 channels in SAN cells. First, $Ca_v1.3$ undergoes VDF particularly during slow heart rate, as channels recover from inactivation. Second, $Ca_v1.3$ channels are strongly colocalized with RYRs. Third, $Ca_v1.2$ channels undergo comparatively little VDF and are not colocalized with sarcomeric RYRs. Thus, despite contributing ~42% of the whole cell $I_{Ca,L}$, $Ca_v1.2$ channels are less capable than $Ca_v1.3$ to restore normal pacemaking. Fourth, a numerical model that included preferential coupling of Cav1.3 channels to RYR-dependent Ca^{2+} release suggests that VDF can promote normal SAN pacemaking. We conclude that differences in VDF and subcellular localization further contribute to the non-overlapping roles of $Ca_v1.2$ and $Ca_v1.3$ in controlling sinus rhythm.

Voltage-dependent facilitation of $Ca_v1.3$ in sinoatrial node cells

Ca_v1 channels undergo frequency-dependent facilitation in multiple cardiac tissues (Lee, 1987; Richard *et al.* 1990; Mangoni *et al.* 2000). The resulting increase in $I_{Ca,L}$ is due in part to CDF. For $Ca_v1.2$, Ca^{2+} influx augments channel open probability through calmodulin (CaM)-dependent protein kinase II (CaMKII) (Dzhura *et al.* 2000; Grueter *et al.* 2006). VDF of $Ca_v1.2$ can also involve CaMKII, but unlike CDF, is seen when Ba^{2+} is used as the permeant ion (Lee *et al.* 2006). While both CDF and VDF have been characterized for $Ca_v1.2$ in ventricular myocytes, little is known regarding these processes for $Ca_v1.3$ in the heart. We focused on I_{Ba} rather than I_{Ca}, as our goal was to

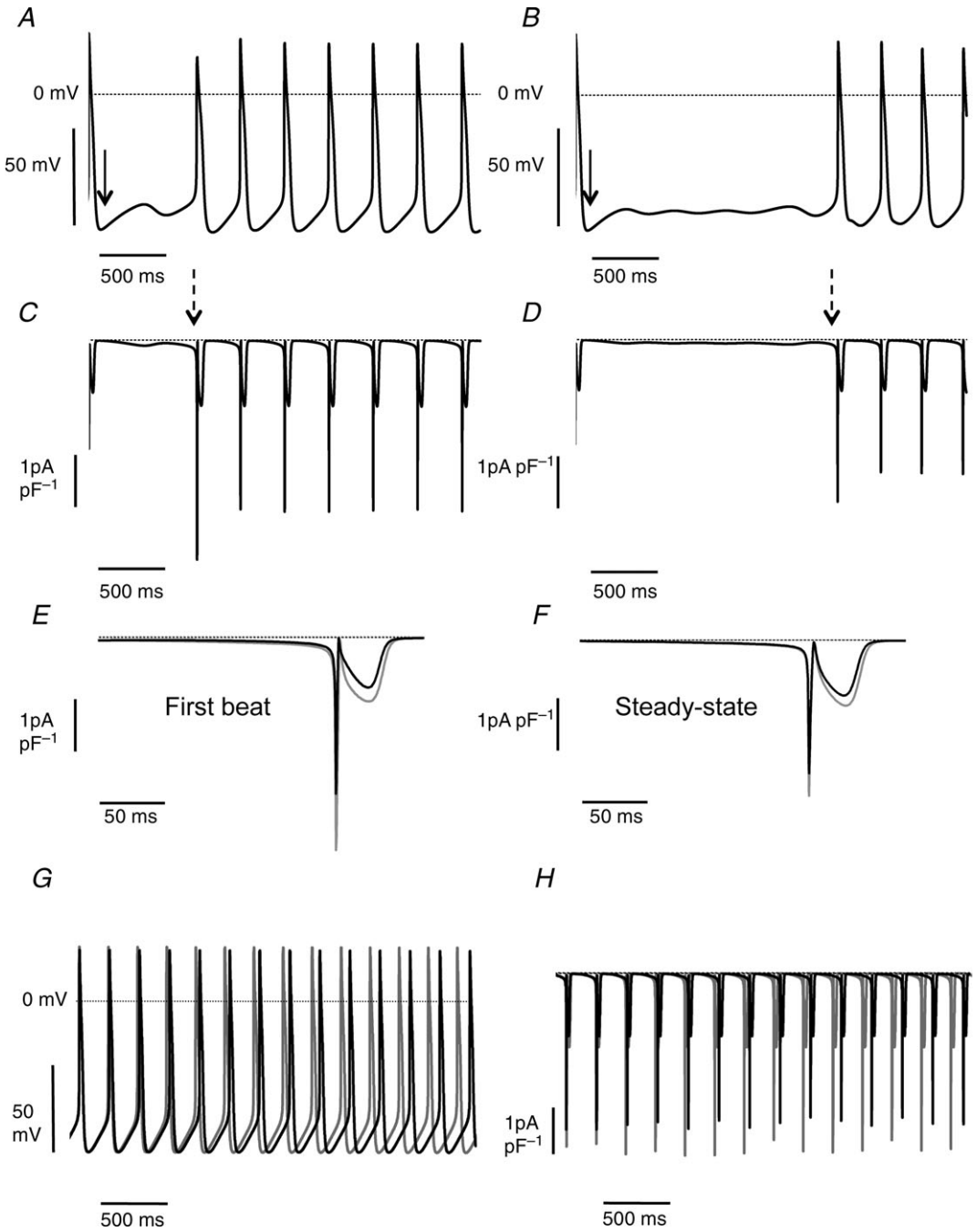

Figure 8. Activation of I_{KATP} transiently stopped automaticity in a model including VDF (*A*) and excluding VDF (*B*)

Arrows indicate the onset of I_{KATP} activation. Pacemaking resumed after pause. At steady state, pacemaker activity was slowed by 18% in the model including VDF and by 20% in the model excluding VDF. *C* and *D* show corresponding $Ca_V1.3$-mediated $I_{Ca,L}$, while dashed arrows indicate $Ca_V1.3$-mediated $I_{Ca,L}$ at the first beat upon resuming of automaticity. *E* and *F*, enlargement of $Ca_V1.3$-mediated $I_{Ca,L}$ at the first beat and steady state upon resuming of automaticity in the model including (grey line) and excluding VDF (black line). Traces represent superimposed $Ca_V1.3$-mediated $I_{Ca,L}$ during steady-state pacemaker activity after I_{KATP} activation in the model including (grey line) and excluding VDF (black line). Steady-state pacemaker activity (*G*) and $Ca_V1.3$-mediated $I_{Ca,L}$ (*H*) after activation of I_{KATP} in the model including VDF (grey line) or after abolition of VDF (black line).

compare VDF of SAN Ca_v1 currents. With Ca^{2+} as the charge carrier, L-type currents undergo CDI, due to CaM, as well as CDF (see Christel & Lee, 2012 for review), both of which would hinder analyses of VDF. Because Ba^{2+} substitutes poorly for Ca^{2+} in binding to CaM (Wang, 1985), voltage-dependent modulation of I_{Ba} can be studied in isolation from Ca^{2+}-dependent modulation.

Using SAN cells from $Ca_v1.2$ DHP mice, we found that VDF for $Ca_v1.3$ $I_{Ba,L}$ is largely consistent with previously described VDF of $I_{Ca,L}$ in rabbit SAN cells (Mangoni *et al.* 2000). Because it was not possible to completely isolate $Ca_v1.3$ VDF from VDI, VDF was only evident following very strong depolarizations (+80 mV; Fig. 4). Our interpretation that VDF is partially obscured by VDI at more negative prepulse voltages is supported by the overt facilitation of $Ca_v1.3$ currents seen at longer intervals after the conditioning prepulse (Fig. 3), assuming that recovery is faster for VDI than VDF. In addition, VDF of $I_{Ca,L}$ was apparent in simulations of voltage-clamp recordings at less positive voltages (+30 mV), compatible with native SAN APs (Fig. 6) and simulated SAN pacemaker activity (Figs 7 and 8).

In comparing the total $I_{Ba,L}$ to the individual $Ca_v1.3$ and $Ca_v1.2$ components, it is clear that one function of $Ca_v1.3$ VDF is to balance the strong VDI of $Ca_v1.2$ in SAN cells (Figs 3 and 4). $Ca_v1.2$ currents showed significant VDI following depolarizing prepulses (~30%), which was offset (~10%) by the limited VDI and stronger VDF of $Ca_v1.3$ currents (Fig. 3). $Ca_v1.3$ VDF also allowed full recovery of $I_{Ba,L}$ within 0.5 s after a strong depolarization (Fig. 4), thus stabilizing $I_{Ba,L}$ from reductions due to $Ca_v1.2$ VDI.

Our finding that $Ca_v1.3$ but not $Ca_v1.2$ undergoes overt VDF during recovery from inactivation (Fig. 2*B*) was unexpected considering that VDF is also a property of $Ca_v1.2$ in transfected cells (Lee *et al.* 2006). VDF of SAN $I_{Ba,L}$ may involve molecular determinants and protein interactions specific for $Ca_v1.3$. For $Ca_v1.3$, the distal C-terminal domain of the long exon 42-containing α_1 subunit contains a type I PDZ binding sequence and autoinhibitory module that suppresses VDF. Binding to PDZ domain-containing proteins such as erbin relieves autoinhibition, resulting in robust VDF in transfected HEK293T cells. $Ca_v1.2$ channels are not subject to such regulation by PDZ domain-containing proteins (Calin-Jageman *et al.* 2007). Whether interactions with erbin or related proteins underlie $Ca_v1.3$-selective VDF in SAN cells remains to be elucidated.

$Ca_v1.3$/ryanodine receptor apposition in sinoatrial node cells

The strong colocalization of $Ca_v1.3$ with RYR2 (Fig. 5) in SAN cells may be relevant for the functional role of RYR-mediated Ca^{2+} release in pacemaking (Vinogradova *et al.* 2002). During the late phase of diastolic depolarization, RYR-mediated Ca^{2+} release promotes activation of a depolarizing current due to Na^+/Ca^{2+} exchange, which accelerates reaching the threshold of the SAN AP upstroke. Close apposition of $Ca_v1.3$ with RYRs may facilitate SR Ca^{2+} release as $I_{Ca,L}$ stimulates RYR open probability. In this respect, numerical simulations predicted that the slope of rise of diastolic RYR-dependent Ca^{2+} release increased as a function of $Ca_v1.3$-mediated $I_{Ca,L}$ half-activation voltage (data not shown). The coupling of this SR Ca^{2+} release to the depolarizing influence of Na^+/Ca^{2+} exchange should accelerate attainment of the threshold for AP firing of SAN cells (Vinogradova *et al.* 2002).

$Ca_v1.3$ channels have been shown to physically associate with RYR2 in the nervous system (Ouardouz *et al.* 2003; Kim *et al.* 2007). However, in neurons, $Ca_v1.3$ activation promotes RYR2-mediated Ca^{2+} release independent of Ca^{2+} influx, suggesting that $Ca_v1.3$ channels may trigger voltage-dependent activation of RYR2 analogous to $Ca_v1.1$ channels and skeletal RYR1 (Paolini *et al.* 2004). Similar characterization of $Ca_v1.3$/RYR interactions will reveal additional insights as to how Ca^{2+}-induced Ca^{2+} release affects automaticity in SAN cells.

$Ca_v1.3$ and arrhythmia

The importance of $Ca_v1.3$ for normal cardiac rhythmicity is now well established. Loss-of-function mutations in the human *CACNA1D* gene encoding $Ca_v1.3$ cause SAN dysfunction and deafness syndrome (SANDD) (Baig *et al.* 2011). Patients with SANDD present with profound deafness and sinus bradycardia, similar to mice with genetic inactivation of *CACNA1D* (Platzer *et al.* 2000). Patients with SANDD also exhibit atrioventricular block and dissociated rhythms, which can be explained by findings that $Ca_v1.3$ is necessary for automaticity of atrioventricular nodal cells (Marger *et al.* 2011). Human mutations in the gene encoding the multifunctional scaffolding protein, ankyrin B, cause reductions in $Ca_v1.3$ current density in SAN cells and atrial myocytes, which is associated with sinus bradycardia and atrial fibrillation, respectively (Le Scouarnec *et al.* 2008; Cunha *et al.* 2011). With respect to defects in $Ca_v1.3$ causing SAN dysfunction, loss of rapid activation kinetics and negative activation thresholds of $Ca_v1.3$ weakens the diastolic depolarization, thus slowing pacemaking (Mangoni *et al.* 2003). By experimental and computational approaches, we establish that VDF and potential coupling with RYRs are additional features of $Ca_v1.3$ that support its role in the generation of heart rhythm.

References

Baig SM, Koschak A, Lieb A, Gebhart M, Dafinger C, Nurnberg G, Ali A, Ahmad I, Sinnegger-Brauns MJ, Brandt N, Engel J, Mangoni ME, Farooq M, Khan HU, Nurnberg P, Striessnig J & Bolz HJ (2011). Loss of Cav1.3 (*CACNA1D*) function in a human channelopathy with bradycardia and congenital deafness. *Nat Neurosci* **14**, 77–84.

Bogdanov KY, Vinogradova TM & Lakatta EG (2001). Sinoatrial nodal cell ryanodine receptor and Na^+-Ca^{2+} exchanger: molecular partners in pacemaker regulation. *Circ Res* **88**, 1254–1258.

Bolte S & Cordelieres FP (2006). A guided tour into subcellular colocalization analysis in light microscopy. *J Microsc* **224**, 213–232.

Calin-Jageman I, Yu K, Hall RA, Mei L & Lee A (2007). Erbin enhances voltage-dependent facilitation of Cav1.3 Ca^{2+} channels through relief of an autoinhibitory domain in the Cav1.3 a1 subunit. *J Neurosci* **27**, 1374–1385.

Christel C & Lee A (2012). Ca^{2+}-dependent modulation of voltage-gated Ca^{2+} channels. *Biochim Biophys Acta* **1820**, 1243–1252.

Cunha SR, Hund TJ, Hashemi S, Voigt N, Li N, Wright P, Koval O, Li J, Gudmundsson H, Gumina RJ, Karck M, Schott JJ, Probst V, Le Marec H, Anderson ME, Dobrev D, Wehrens XH & Mohler PJ (2011). Defects in ankyrin-based membrane protein targeting pathways underlie atrial fibrillation. *Circulation* **124**, 1212–1222.

Dzhura I, Wu Y, Colbran RJ, Balser JR & Anderson ME (2000). Calmodulin kinase determines calcium-dependent facilitation of L-type calcium channels. *Nat Cell Biol* **2**, 173–177.

Fukuzaki K, Sato T, Miki T, Seino S & Nakaya H (2008). Role of sarcolemmal ATP-sensitive K^+ channels in the regulation of sinoatrial node automaticity: an evaluation using Kir6.2-deficient mice. *J Physiol* **586**, 2767–2778.

Gregory FD, Bryan KE, Pangrsic T, Calin-Jageman IE, Moser T & Lee A (2011). Harmonin inhibits presynaptic Cav1.3 Ca^{2+} channels in mouse inner hair cells. *Nat Neurosci* **14**, 1109–1111.

Grueter CE, Abiria SA, Dzhura I, Wu Y, Ham AJ, Mohler PJ, Anderson ME & Colbran RJ (2006). L-type Ca^{2+} channel facilitation mediated by phosphorylation of the b subunit by CaMKII. *Mol Cell* **23**, 641–650.

Hoesl E, Stieber J, Herrmann S, Feil S, Tybl E, Hofmann F, Feil R & Ludwig A (2008). Tamoxifen-inducible gene deletion in the cardiac conduction system. *J Mol Cell Cardiol* **45**, 62–69.

Jenkins MA, Christel CJ, Jiao Y, Abiria S, Kim KY, Usachev YM, Obermair GJ, Colbran RJ & Lee A (2010). Ca2+-dependent facilitation of Cav1.3 Ca2+ channels by densin and Ca2+/calmodulin-dependent protein kinase II. *JNeurosci* **30**, 5125–5135.

Kharche S, Yu J, Lei M & Zhang H (2011). A mathematical model of action potentials of mouse sinoatrial node cells with molecular bases. *Am J Physiology Heart Circ Physiol* **301**, H945–963.

Kim S, Yun HM, Baik JH, Chung KC, Nah SY & Rhim H (2007). Functional interaction of neuronal Cav1.3 l-type calcium channel with ryanodine receptor type 2 in the rat hippocampus. *J Biol Chem* **282**, 32877–32889.

Klugbauer N, Welling A, Specht V, Seisenberger C & Hofmann F (2002). L-type Ca^{2+} channels of the embryonic mouse heart. *Eur J Pharmacol* **447**, 279–284.

Koschak A, Reimer D, Huber I, Grabner M, Glossmann H, Engel J & Striessnig J (2001). a1D (Cav1.3) subunits can form L-type Ca^{2+} channels activating at negative voltages. *J Biol Chem* **276**, 22100–22106.

Kurata Y, Hisatome I, Imanishi S & Shibamoto T (2002). Dynamical description of sinoatrial node pacemaking: improved mathematical model for primary pacemaker cell. *Am J Physiol Heart Circ Physiol* **283**, H2074–2101.

Le Scouarnec S, Bhasin N, Vieyres C, Hund TJ, Cunha SR, Koval O, Marionneau C, Chen B, Wu Y, Demolombe S, Song LS, Le Marec H, Probst V, Schott JJ, Anderson ME & Mohler PJ (2008). Dysfunction in ankyrin-B-dependent ion channel and transporter targeting causes human sinus node disease. *Proc Natl Acad Sci U S A* **105**, 15617–15622.

Lee A, Scheuer T & Catterall WA (2000). Ca^{2+}/calmodulin-dependent facilitation and inactivation of P/Q-type Ca^{2+} channels. *J Neurosci* **20**, 6830–6838.

Lee A, Wong ST, Gallagher D, Li B, Storm DR, Scheuer T & Catterall WA (1999). Ca^{2+}/calmodulin binds to and modulates P/Q-type calcium channels. *Nature* **399**, 155–159.

Lee KS (1987). Potentiation of the calcium-channel currents of internally perfused mammalian heart cells by repetitive depolarization. *Proc Natl Acad Sci U S A* **84**, 3941–3945.

Lee TS, Karl R, Moosmang S, Lenhardt P, Klugbauer N, Hofmann F, Kleppisch T & Welling A (2006). Calmodulin kinase II is involved in voltage-dependent facilitation of the L-type Cav1.2 calcium channel: Identification of the phosphorylation sites. *J Biol Chem* **281**, 25560–25567.

Lei M, Jones SA, Liu J, Lancaster MK, Fung SS, Dobrzynski H, Camelliti P, Maier SK, Noble D & Boyett MR (2004). Requirement of neuronal- and cardiac-type sodium channels for murine sinoatrial node pacemaking. *J Physiol* **559**, 835–848.

Maltsev VA & Lakatta EG (2009). Synergism of coupled subsarcolemmal Ca^{2+} clocks and sarcolemmal voltage clocks confers robust and flexible pacemaker function in a novel pacemaker cell model. *Am J Physiol Heart Circ Physiol* **296**, H594–615.

Mangoni ME, Couette B, Bourinet E, Platzer J, Reimer D, Striessnig J & Nargeot J (2003). Functional role of L-type Cav1.3 Ca^{2+} channels in cardiac pacemaker activity. *Proc Natl Acad Sci U S A* **100**, 5543–5548.

Mangoni ME, Couette B, Marger L, Bourinet E, Striessnig J & Nargeot J (2006*a*). Voltage-dependent calcium channels and cardiac pacemaker activity: From ionic currents to genes. *Prog Biophys Mol Biol* **90**, 38–63.

Mangoni ME, Fontanaud P, Noble PJ, Noble D, Benkemoun H, Nargeot J & Richard S (2000). Facilitation of the L-type calcium current in rabbit sino-atrial cells: effect on cardiac automaticity. *Cardiovasc Res* **48**, 375–392.

Mangoni ME & Nargeot J (2001). Properties of the hyperpolarization-activated current (I_f) in isolated mouse sino-atrial cells. *Cardiovasc Res* **52**, 51–64.

Mangoni ME, Traboulsie A, Leoni AL, Couette B, Marger L, Le Quang K, Kupfer E, Cohen-Solal A, Vilar J, Shin HS, Escande D, Charpentier F, Nargeot J & Lory P (2006*b*). Bradycardia and slowing of the atrioventricular conduction in mice lacking $Ca_V3.1/\alpha_{1G}$ T-type calcium channels. *Circ Res* **98**, 1422–1430.

Marger L, Mesirca P, Alig J, Torrente A, Dubel S, Engeland B, Kanani S, Fontanaud P, Striessnig J, Shin HS, Isbrandt D, Ehmke H, Nargeot J & Mangoni ME (2011). Functional roles of Cav1.3, Cav3.1 and HCN channels in automaticity of mouse atrioventricular cells: insights into the atrioventricular pacemaker mechanism. *Channels* **5**, 251–261.

Marionneau C, Couette B, Liu J, Li H, Mangoni ME, Nargeot J, Lei M, Escande D & Demolombe S (2005). Specific pattern of ionic channel gene expression associated with pacemaker activity in the mouse heart. *J Physiol* **562**, 223–234.

Neco P, Torrente AG, Mesirca P, Zorio E, Liu N, Priori SG, Napolitano C, Richard S, Benitah JP, Mangoni ME & Gomez AM (2012). Paradoxical effect of increased diastolic Ca^{2+} release and decreased sinoatrial node activity in a mouse model of catecholaminergic polymorphic ventricular tachycardia. *Circulation* **126**, 392–401.

Olson PA, Tkatch T, Hernandez-Lopez S, Ulrich S, Ilijic E, Mugnaini E, Zhang H, Bezprozvanny I & Surmeier DJ (2005). G-protein-coupled receptor modulation of striatal $Ca_V1.3$ L-type Ca^{2+} channels is dependent on a Shank-binding domain. *J Neurosci* **25**, 1050–1062.

Ouardouz M, Nikolaeva MA, Coderre E, Zamponi GW, McRory JE, Trapp BD, Yin X, Wang W, Woulfe J & Stys PK (2003). Depolarization-induced Ca^{2+} release in ischemic spinal cord white matter involves L-type Ca^{2+} channel activation of ryanodine receptors. *Neuron* **40**, 53–63.

Paolini C, Fessenden JD, Pessah IN & Franzini-Armstrong C (2004). Evidence for conformational coupling between two calcium channels. *Proc Natl Acad Sci U S A* **101**, 12748–12752.

Platzer J, Engel J, Schrott-Fischer A, Stephan K, Bova S, Chen H, Zheng H & Striessnig J (2000). Congenital deafness and sinoatrial node dysfunction in mice lacking class D L-type Ca^{2+} channels. *Cell* **102**, 89–97.

Richard S, Tiaho F, Charnet P, Nargeot J & Nerbonne JM (1990). Two pathways for Ca^{2+} channel gating differentially modulated by physiological stimuli. *Am J Physiol Heart Circ Physiol* **258**, H1872–H1881.

Rigg L, Heath BM, Cui Y & Terrar DA (2000). Localisation and functional significance of ryanodine receptors during beta-adrenoceptor stimulation in the guinea-pig sino-atrial node. *Cardiovasc Res* **48**, 254–264.

Scholze A, Plant TD, Dolphin AC & Nurnberg B (2001). Functional expression and characterization of a voltage-gated CaV1.3 (a1D) calcium channel subunit from an insulin-secreting cell line. *Mol Endocrinol* **15**, 1211–1221.

Seisenberger C, Specht V, Welling A, Platzer J, Pfeifer A, Kuhbandner S, Striessnig J, Klugbauer N, Feil R & Hofmann F (2000). Functional embryonic cardiomyocytes after disruption of the L-type alpha1C (Cav1.2) calcium channel gene in the mouse. *J Biol Chem* **275**, 39193–39199.

Sinnegger-Brauns MJ, Hetzenauer A, Huber IG, Renstrom E, Wietzorrek G, Berjukov S, Cavalli M, Walter D, Koschak A, Waldschutz R, Hering S, Bova S, Rorsman P, Pongs O, Singewald N & Striessnig JJ (2004). Isoform-specific regulation of mood behaviour and pancreatic beta cell and cardiovascular function by L-type Ca^{2+} channels. *J Clin Invest* **113**, 1430–1439.

Tadross MR, Ben Johny M & Yue DT (2010). Molecular endpoints of Ca^{2+}/calmodulin- and voltage-dependent inactivation of $Ca_V1.3$ channels. *J Gen Physiol* **135**, 197–215.

Tippens AL, Pare J-F, Langwieser N, Moosmang S, Milner TA, Smith Y & Lee A (2008). Ultrastructural evidence for pre- and post-synaptic localization of Cav1.2 l-type Ca^{2+} channels in the rat hippocampus. *J Comp Neurol* **506**, 569–583.

Vinogradova TM, Bogdanov KY & Lakatta EG (2002). beta-Adrenergic stimulation modulates ryanodine receptor Ca^{2+} release during diastolic depolarization to accelerate pacemaker activity in rabbit sinoatrial nodal cells. *Circ Res* **90**, 73–79.

Wang CL (1985). A note on Ca^{2+} binding to calmodulin. *Biochem Biophys Res Commun* **130. 130**, 426–430.

Xu W & Lipscombe D (2001). Neuronal Cav1.3 a1 L-type channels activate at relatively hyperpolarized membrane potentials and are incompletely inhibited by dihydropyridines. *J Neurosci* **21**, 5944–5951.

Zhang H, Fu Y, Altier C, Platzer J, Surmeier DJ & Bezprozvanny I (2006). $Ca_V1.2$ and $Ca_V1.3$ neuronal L-type calcium channels: differential targeting and signalling to pCREB. *Eur J Neurosci* **23**, 2297–2310.

Zhang H, Maximov A, Fu Y, Xu F, Tang TS, Tkatch T, Surmeier DJ & Bezprozvanny I (2005). Association of $Ca_V1.3$ l-type calcium channels with Shank. *J Neurosci* **25**, 1037–1049.

Zhang J, Berra-Romani R, Sinnegger-Brauns MJ, Striessnig J, Blaustein MP & Matteson DR (2007). Role of Cav1.2 l-type Ca^{2+} channels in vascular tone: effects of nifedipine and Mg^{2+}. *Am J Physiol Heart Circ Physiol* **292**, H415–425.

Zhang Q, Timofeyev V, Qiu H, Lu L, Li N, Singapuri A, Torado CL, Shin HS & Chiamvimonvat N (2011). Expression and roles of Cav1.3 (α_{1D}) L-type Ca^{2+} channel in atrioventricular node automaticity. *J Mol Cell Cardiol* **50**, 194–202.

Author contributions

The experiments in this study were performed at the University of Iowa, University of Montpellier, and University of Erlangen. Specific contributions are as follows: conception and design of experiments: C.J.C., P.M., S.H., M.E.M. and Amy Lee; collection, analysis, and interpretation of data: C.J.C., N.C., P.M., S.H., M.E.M. and A.L.; drafting the article or revising it critically for important intellectual content: C.J.C., M.E.M., S.H., A.L., J.S. and A.L. All authors approved the final version of the manuscript.

Acknowledgements

Supported by the NIH (DC009433, HL087120 to A.L.; T32007121 to C.J.C.), the Carver Research Program of Excellence (to A.L.), Deutsche Forschungsgemeinschaft (GRK 333 to A. Ludwig), Austrian Science Fund (P20670 to J.S.), ANR-2010-BLAN-1128-01 and ANR-09-GENO-034 (to M.E.M.). The IGF group is a member of the Laboratory of Excellence 'Ion Channel Science and Therapeutics' supported by a grant from ANR. The authors thank Dr Yuejin Wu for advice with SAN cell recording and Dr Mark Anderson for comments on the manuscript.